Intestinal barrier breakdown and mucosal microbiota disturbance in neuromyelitis optical spectrum disorder

Chunping Cui
Third Affiliated Hospital of Sun Yat-Sen University
Sha Tan
Third Affiliated Hospital of Sun Yat-Sen University
Li Tao
Third Affiliated Hospital of Sun Yat-Sen University
Junli Gong
Sun Yat-sen University Sixth Affiliated Hospital
Yanyu Chang
Third Affiliated Hospital of Sun Yat-Sen University
Yuge Wang
Third Affiliated Hospital of Sun Yat-Sen University
Ping Fan
Third Affiliated Hospital of Sun Yat-Sen University
Dan He
Third Affiliated Hospital of Sun Yat-Sen University
Yiwen Ruan
Jinan University
Wei Qiu (qiuwei120@vip.163.com)
Third Affiliated Hospital of Sun Yat-Sen University https://orcid.org/0000-0002-0880-958X

Research

Keywords: Neuromyelitis optica sectrum disorders, tight junction, intestinal barrier, mucosa microbiota

Posted Date: April 24th, 2020

DOI: https://doi.org/10.21203/rs.3.rs-22503/v1

Version of Record: A version of this preprint was published at Frontiers in Immunology on September 2nd, 2020. See the published version at https://doi.org/10.3389/fimmu.2020.02101.

Abstract

Background and purpose

The mechanism underlying the pathology of neuromyelitis optica spectrum disorder (NMOSD) remains unclear even though increased expression of the water channel protein aquaporin-4 (AQP4) on astrocytes plays an important role. Our previous study revealed that dysbiosis was detected in the faecal microbiota of NMOSD patients. In this study, we further investigated whether the intestinal barrier and mucosal flora balance were also interrupted in NMOSD patients.

Methods

Sigmoid mucosal biopsies were collected via endoscopy from six patients with NMOSD and compared with those from three patients with multiple sclerosis (MS) and five healthy controls (HCs). These samples were processed for electron microscopy and immunohistochemistry to investigate changes in ultrastructure and in the number and size of intestinal inflammatory cells. Changes in mucosal flora were also analysed by high-throughput 16S ribosomal RNA gene amplicon sequencing.

Results

The intercellular space between epithelia of the colonic mucosa became wider in MS and NMOSD patients compared to the HCs ($P < 0.01$), and the expression of tight junction proteins in MS and NMOSD patients significantly decreased compared to that in the HCs. Activation of microphages with many inclusions inside the cytoplasm and enlarged plasmocytes with more particles were found in the NMOSD group. Quantitative analysis showed that the percentage of small-size CD 38 + and CD138 + cells was lower but that of larger-size cells became higher in NMOSD patients, and 16S data showed that the abundance of *Streptococcus* and *Granulicatella* was dramatically increased in NMOSD patients.

Conclusions

NMOSD patients exhibited a disrupted intestinal barrier and intestinal dysbiosis and activation of intestinal inflammation, which suggested a potential pathophysiological mechanism of NMOSD underlying intestinal inflammation.

Introduction

Neuromyelitis optica spectrum disorder (NMOSD) is recognized as a distinct clinical entity from multiple sclerosis (MS) based on the disease-specific serum autoantibody aquaporin-4 (AQP4)-IgG. Molecular mimicry, which can occur when a foreign protein that shares structural or amino-acid sequence homology with a self-antigen elicits cross-reactive immunity, is implicated in the pathogenesis of several

rheumatologic and autoimmune disorders in the central nervous system (CNS). One search of bacterial and viral proteins revealed extensive homology in NMOSD[1]. The brain-gut axis reveals multiple and complicated connections among the gut microbiota, intestinal barrier and immune system in autoimmune diseases[2]. Pathogenic bacteria and their abnormal metabolites can directly cause an abnormal number of immune cells in the intestinal mucosa[3]. In addition, the intestinal microbiota can indirectly influence intestinal inflammation by damaging the intestinal barrier. Since tight junction (TJ) proteins are the major ingredients of the intestinal barrier, commensal bacteria may enter the lamina propria, leading to pathological consequences after the TJ proteins and epithelial barrier are breached[4].

Several studies[5–7] have reported that faecal microbes may not accurately represent the engraftment colony in the gastrointestinal tract. The microbiota of the intestinal mucosa and faeces as well as their relevance to diseases are largely different. For example, data from patients with inflammatory bowel diseases or chronic constipation[6] suggested that the evaluation of the mucosal microbiota is better than that of faecal microbiota. Recently, our group[8, 9] and others[10, 11] reported that faecal microbiota were associated with the severity of NMOSD and MS. However, the role of the mucosal microbiota and intestinal barrier in NMOSD remains unclear. In the present study, we further investigated the pathological changes in the colonic mucosa, including the intestinal barrier, mucosal flora and inflammatory response, in NMOSD patients.

Methods

2.1 Research participants

Six Chinese NMOSD patients who fulfilled the criteria of Wingerchuk and were seropositive for AQP4-IgG were consecutively recruited from the Multiple Sclerosis Center. Three Chinese MS patients fulfilling the McDonald diagnostic criteria[13] were enrolled as controls, and five healthy controls (HCs) were recruited from the Health Examination Center of the Third Affiliated Hospital, Sun Yat-sen University, from July 2019 to October 2019. The participants in the patient group had no history of intravenous methylprednisolone therapy or disease-modifying therapies for six months. The control group was matched for body mass index (BMI), age, and sex. Subjects consuming probiotics or antibiotics within 1 month before admission were excluded. The severity of NMOSD and MS subjects was assessed using the Expanded Disability Status Scale (EDSS) score, which was divided into three classes (< 3,3–5, > 5).

The present research was approved by the ethics committee of the Third Affiliated Hospital of Sun Yat-sen University. Informed written consent was obtained from the patients.

2.2 Mucosal Specimen Collection

Previous studies[14, 15] reported that there was no significant difference in the microbiota associated with ileal, caecal and rectal mucosa. Sigmoid mucosal biopsies were collected via endoscopy in the present study. A limited, prepped sigmoidoscopy was performed using a standard adult fibro-

colonoscope to 20–25 cm from the anal verge. Biopsies were taken from pink mucosa without visible faeces at the sigmoid colon approximately 20 cm from the anal verge and were either snap frozen at -80 °C or processed with 2.5% glutaric dialdehyde, protein preservation solution (Kingmed Diagnostics, Guangzhou, China) and 10% formalin fixation in the endoscopy room.

2.3 Electron Microscopy And Data Analysis

After washing in phosphate buffered saline solution, the sample was placed in osmium tetroxide for 2 h. Then, the samples were dehydrated in a series of ethanol solutions of increasing concentrations until 100%, infiltrated with propylene oxide, embedded in pure resin (Epon812, TED PELLA, America) and solidified. Localization of the mucosa was obtained under an Olympus optical microscope (model: BX41, Olympus, Hamburg, Germany), and then 1-micron thick semi-thin sections were cut under a Leica ultrathin microtome (model: UC-7, Leica Microsystems, Wetzlar, Germany). After the tissue of the whole section was observed, ultrathin sections (50–70 nm) were cut on the same microtome. The ultrathin sections were stained with 2% uranium dioxide acetate (SPI Supplies, West Chester, America) and lead citrate (TED PELLA, America). Images were observed and obtained under a transmission electron microscope (JEM-1400 PLUS, Japan Electron Optics Laboratory Co., Ltd, Japan).

2.4 Immunofluorescence Staining

Sigmoid colon mucosal specimens were postfixed in protein preservation fixative (Kingmed Diagnostics, Guangzhou, China) and then washed twice with protein preservation cleaning solution (Kingmed Diagnostics, Guangzhou, China) for 10 min each. Sections of 4 μm were cut from frozen mucosa on a cryostat (serial no. 0325; Thermo Scientific, Cheshire, UK) and fixed in 4℃ acetone for 10 min. A circle was drawn around the sections on a slide by a Dako pen (code no. S2002; Dako, Glostrup, Denmark) to prevent the antibody from flowing out. Then, the sections were incubated for 40 min at 37 °C with primary antibodies against zonula occludens-1 (ZO-1) (rabbit anti-ZO1 antibody 1:50, Abcam, ab96587), occludin (OCC) (rabbit anti-occludin antibody 1:50, Abcam, ab235986), and claudin-1 (CLA) (rabbit anti-claudin 1 antibody 1:50, Abcam, ab15098) separately. After washing in 0.01 M PBS 3 times for 5 min each, the sections were incubated with Alexa Fluor-conjugated secondary antibody (Goat Anti-Rabbit IgG H&L 1:400, Abcam, ab150077). Finally, the sections were covered with glycerine and a glass coverslip.

2.5 Immunohistochemistry

All biopsy samples from the HCs and NMOSD and MS patients were processed for immunohistochemical staining to detect antigens of CD3, CD20, CD38, CD68, and CD138. Blocks of colonic mucosa were fixed by formalin, embedded in paraffin and then cut into 4 μm thick sections. After xylene dewaxing, gradient ethanol rehydration and high-pressure antigen retrieval, tissue sections were stained with the selected streptavidin–biotin–peroxidase (SP) staining method. Guided by the Novolink Detection Kit instructions

(Leica Novocastra, Re7280-k, Germany), the following operations were carried out: all sections were treated with primary antibodies at 4 °C overnight. These antibodies included anti-CD3 and anti-CD20 antibodies (1:200, from rabbit, Dako Denmark, Glostrup, Denmark) and anti-CD38 (1:400), anti-CD68 (1:800), and anti-CD138 (1:600) antibodies (from rabbit, Leica Microsystems, Deerfield, IL, USA). Then, these sections were incubated with biotin-conjugated anti-rabbit secondary antibody for 30 min at 37 °C followed by the enzyme substrate 3',3-diaminobenzidine tetrahydrochloride (DAB reagent kit, Re7163, Germany) for colour development. Images were observed and obtained by an Olympus microscope (model: BX43, Olympus, Hamburg, Germany).

2.6 Quantitative Analysis

2.6.1 Analysis of intercellular spaces

Fluorescent images were taken using a Zeiss confocal microscope (LSM700, Zeiss, Germany), and images in different channels were overlaid using Adobe Photoshop (v. CS3, Adobe, San Jose, CA) software. The intercellular space, including TJs, adhering junctions and desmosomes between two epithelial cells, was measured randomly from 5 pictures per specimen by ImageJ. An intercellular space was defined as the gap from one border of one epithelium to another border of the adjacent epithelium, excluding the dense adherent structures. The measurement was performed by double blinding.

2.6.2 Analysis of the density and size of inflammatory cells

(1) The density of inflammatory cells: In the present study, we employed 5 antibodies to detect the activation of inflammation: CD3, a marker for T lymphocytes; CD20, a marker for B lymphocytes; CD38, expressed on B lymphocytes and plasma cells; CD68, a marker for monocytes and macrophages; and CD138, a marker for plasma cells. The density and percentage of infiltrated inflammatory cells were assessed according to the methods described by Ma et al.[16]. First, the density of positive cells was determined by immunohistochemical staining colour and graded as 4 levels: 0 (no colour), 1 (light yellow), 2 (light brown), and 3 (brown). Second, the number of positive cells (the percentage of area covered by coloured cells/image area) was graded as 0 (< 5%), 1 (5–25%), 2 (25–50%), 3 (51–75%), or 4 (> 75%). Third, the two grades were then added together, and the grade scores were used to evaluate the inflammatory reaction of the colonic mucosa in each group. Inflammatory infiltrates were graded as 0 (no inflammatory cell infiltration), 1 (mild inflammatory cell infiltration), 2 (moderate inflammatory cell infiltration or < 50 aggregated inflammatory cells), 3 (> 50 aggregated inflammatory cells as an organized “focus”), and 4 (more than one focus). A representative section was evaluated for each sample by two skilled pathologists at different times, averaging the scores.

(2) The size of inflammatory cells

We randomly selected 30–50 CD3-, CD20-, CD38-, CD68-, and CD138-positive cells from each specimen and measured the area of these cells at high power (X400) to assess the cell functional status by ImageJ (National Institutes of Health, USA, Version 1.51 k). Based on the data of the area, we classified these cells into five levels and made comparisons among the different levels of cells.

2.7 Microbiota Analysis

Bacterial DNA was extracted from colonic mucosal samples with the QIAamp Power Fecal DNA Kit (Qiagen, Germany) according to the manufacturer's instructions. Construction of sequencing libraries and paired sequencing (2 × 250 bp) was performed on an Illumina MiSeq platform at Biomarker Technologies Co, Ltd (Beijing, China) according to standard protocols. Custom Perl and Bash scripts were used to demultiplex the reads and assign barcoded reads to individual samples. Reads were kept only when the sequence included a perfect match to the barcode and the V4 16S rRNA gene primers and were within the length expected for the V3–V4 variable region. The raw data were merged using FLASH[17]. Sequences were quality filtered using Trimmomatic[18], and chimaera sequences were removed using a UCHIME algorithm[19].

2.8 Statistical Analysis

Statistical analysis was performed in SPSS (version 20.0) and GraphPad Prism 6.0 software. After passing equal variance testing, the intercellular spaces, immunohistochemical intensity staining scores and average optical density (AOD) of CLA, OCC, and ZO-1 were analysed by the Kruskal-Wallis test, and the size of cells was analysed by the T-test. All data are presented as the mean ± SEM. α-diversity (Chao1 richness estimator, Shannon-Wiener diversity index, Simpson diversity index) was calculated based on rarefied operational taxonomic unit (OTU) counts. Principal coordinate analysis (PCoA) was coordinated from the weighted UniFrac distance; the linear discriminant analysis (LDA) effect size (LEfSe) pipeline[20] and Metastats[21] were employed to differentially identify microbes that distinguished patients from HCs. The effective sequences were binned into OTUs using USEARCH software with a cut-off of 97% identity in 16S[22]. A value of $p < 0.05$ was considered statistically significant in the compared groups.

Results

3.1 Information collected from HCs and from MS and NMOSD subjects

Information regarding the number, sex, age, BMI, AQP4-IgG status, and disease severity of all subjects is presented in Table 1.

Table 1
Demographic and clinical features of NMOSD, MS and HCs.

	NMOSD	MS	HCs	p-value
N	6	3	5	
Female, n (%)	6 (100%)	3 (100%)	5(100%)	
Age, years	41.67 ± 14.95	30.67 ± 7.09	36.40 ± 11.26	0.475
BMI, kg/m2	21.19 ± 3.49	23.82 ± 3.08	20.95 ± 2.08	0.396
AQP4-IgG, n (%)	6(100%)	-	-	
Disease severity	2 (33.33%)	3(100%)		
EDSS	1 (16.67%)	0		
< 3	3 (50.00%)	0		
3–5				
> 5				

NMOSD: neuromyelitis optica spectrum disorders; MS: mutiple sclerosis; HCs: healthy controls; BMI: body mass index; AQP4: aquaporin-4; EDSS:Expanded Disability Status Scale; IgG: Immunoglobulin G.

3.2 The width of intercellular spaces increased in the colonic mucosa of MS and NMOSD patients

Our previous studies have shown a disturbance in the flora of faeces of MS and NMOSD patients, with *Streptococcus* being dominant[8, 9]. Because these bacteria can produce streptococcal toxin, which is harmful to human cells and tissues[23], we hypothesized that streptococcal toxin produced by *Streptococcus* in the intestine may first attack the epithelium of mucosa because epithelial cells directly contact the contents of the lumen of the intestine. Epithelial cells are connected by gap junctions, which ensure epithelial barrier integrity and regulate paracellular permeability. Therefore, in the present study, we employed electron microscopy to investigate changes in intercellular space. Under an electron microscope (EM), we observed three typical types of gap junctions between two adjacent epithelia of the colonic mucosa in all subjects: TJs, adherent junctions (AJs) and desmosomes (Fig. 1A, arrows). The TJ was located nearest the lumen, and the gap space was narrow (Fig. 1A, B & C). Compared to the HC and MS subjects, some TJs of NMOSD patients were separated (Fig. 1C, arrow). The AJ featured a wider gap space and linear densifications along parts of the junction (Fig. 1A, B & C). The desmosomes were characterized by a wider intercellular space and dense plates on each side of the desmosome (Fig. 1A). From the EM photos, we found that many dense plates of desmosomes became pale or lost when comparing HC and MS subjects (Fig. 1A, B & C, asterisks). The quantitative analysis data showed that the

width of the intercellular space was significantly increased in MS (61.71 ± 5.10 nm) and NMOSD (47.78 ± 2.90 nm) patients compared with HC (35.72 ± 2.09 nm) subjects ($p < 0.01$) (Fig. 1D).

3.2.2 Protein expression of TJs decreased in the colonic mucosa of MS and NMOSD patients

The integrity and permeability of TJs are regulated by several important proteins, such as OCC, CLA and ZO-1. Therefore, we used immunofluorescence staining methods to investigate the expression of these proteins in different groups. Photomicrographs displayed positive staining for OCC, CLA and ZO-1 (Fig. 2, Green). In the HC group, the distribution of OCC and CLA was at the epithelial surface and intercellular space between epithelia of the colonic mucosa ((Fig. 2B). A1 & B1, arrows). However, the expression of these two proteins in the intercellular space was barely detected ((Fig. 2B). A2 & B2), and only weak positive signals were found in the epithelial surface of the colonic mucosa ((Fig. 2B). A3 & B3, arrows) in the MS and NMOSD groups. Interestingly, ZO-1 was expressed only on the epithelial surface and the intercellular space, even in the HC group ((Fig. 2B). C1, arrow), and weak positive signals occurred in MS and NMOSD patients ((Fig. 2C). C2& C3, arrows). Consistent with the observation under confocal microscopy, quantitative analyses showed that a dramatic decrease in OCC levels occurred in the MS (AOD: 0.1104 ± 0.0069) and NMOSD (0.0854 ± 0.0772) groups when compared to the HC group (0.3185 ± 0.0281), both $p < 0.01$ (Fig. 2A4). The expression of CLA in the MS (AOD: 0.1754 ± 0.0558) and NMOSD (0.2778 ± 0.0471) groups was also decreased when compared with that in the HC group (0.4609 ± 0.0353), both $p < 0.01$ (Fig. 2B4). Similarly, the ZO-1 level in the MS (AOD: 0.0765 ± 0.0063) and NMOSD (0.0899 ± 0.0059) groups was also lower than that in the HC group (0.3271 ± 0.0270), both $p < 0.01$ (Fig. 2C4).

3.3 Activation of inflammatory cells in MS and NMOSD patients

When the epithelial barrier is damaged, toxins, such as streptococcal toxins[23], from harmful bacteria elicit an inflammatory pathology of the colonic mucosa. Therefore, we further investigated changes in inflammatory cells of the lamina proper of the colonic mucosa in all subsets of the three groups. Under transmission electron microscopy (TEM), we observed that the normal lymphocytes had a dentate-like nucleus with abundant dense heterochromatins forming aggregates close to the membrane (Fig. 3A (l)). Plasma cells have a spherical nucleus surrounded by a pale zone (Fig. 3A (arrows)) with abundant rough endoplasmic reticulum in the cytoplasm (Fig. 3A (asterisks)). In MS patients, we also observed lymphocytes (Fig. 3B (l)) and plasma cells (Fig. 3B (P)). In addition, we found that macrophages engulfed many dense bodies (Fig. 3B (mac)) and fibrocytes with a longer and curved cytoplasmic tail (Fig. 3B (fib, asterisks)). Some of the fibrocytes underwent an apoptotic process, showing an interrupted cytoplasmic tail (Fig. 3B (arrows)). For NMOSD patients, we found more macrophages with burdened inclusions of different sizes (Fig. 3C & D (mac, asterisks)). In NMOSD patients, we also found eosinophils with larger

and dense granules in the cytoplasm (Fig. 3C (eos, asterisks)), and plasma cells became larger with some vesicles (Fig. 3D (P, arrows)).

Next, we employed immunohistochemistry staining to detect changes in inflammatory cells with five antibodies. As shown in Fig. 4, the three columns in Fig. 4 represent the HC, MS and NMOSD groups, respectively, and the five transverse rows represent the CD3-positive cells (T lymphocytes, Fig. 4A1, A2&A3); CD20-positive cells (B lymphocytes, Fig. 4B1, B2 & B3); CD38-positive cells (B lymphocytes and plasma cells, Fig. 4C1, C2 & C3); CD68-positive cells (monocytes and macrophages, Fig. 4C). D1, D2 & D3); and CD138-positive cells (plasma cells, Fig. 4E1, E2 & E3).

The following step was to perform a semiquantitative analysis to determine the inflammatory response by measuring the colour intensity of immunostaining. The results are shown in Table 2. The score number in Table 2 indicates the severity of inflammation: the higher the number is, the more severe the inflammation. Unfortunately, there was no significant difference among subjects in the three groups by the method. To obtain more detailed and more accurate information from these immunostaining-positive cells, we randomly selected 30–50 cells of each type in each group to draw their areas by ImageJ. From Fig. 5, we found a trend that the mean area of each type of cell increased in MS or NMOSD patients or both but that there were no significant differences except CD138-positive cells, which markedly increased in the MS group (2151 ± 123 μm^2) and in the NMOSD group (2225 ± 149 μm^2) when compared with the HC group (1817 ± 40 μm^2), $p < 0.05$ (Fig. 5A1, B1, C1, D1, &E1). When we separated the cells into different levels based on the size of the area, we found that the percentage of small (500–1000 μm^2) CD3-positive cells in the MS (15.2%±7.6) and NMOSD (29.0%±7.2) groups was significantly lower than that in the HC group (50.6%±5.5), $p < 0.05$, while the percentage of larger (> 2000 μm^2) CD3-positive cells in NMOSD patients (16%±11.5) was higher than that in HC subjects (1.9%±1.5), although there was no significant difference $p > 0.05$ (Fig. 5A2). However, the percentage of small (1000–2000 μm^2) CD38-positive cells (23.2.5%±3.8) and CD138-positive cells (41.3%±5.5) was markedly lower in the NMOSD group than in the HC group (41.0% 6.8 and 63.5%±3.6, respectively), both $p < 0.05$ (Fig. 5C2 & E2). In contrast, the percentages of larger (2000–3000 μm^2) CD38-positive cells in NMOSD (47.5%±3.3) vs HC (36.5%±3.8%) subjects and of CD138-positive cells in NMOSD (40%±1.7) vs HC (29.1%±1.8) subjects were significantly increased, both $p < 0.05$. The percentage of the largest (> 4000 μm^2) CD38-positive cells in NMOSD vs HC was 13%±4.4 vs 1.0%±0.6, and that of CD138-positive cells was 2.3%±1.0 vs 0%±0), both $p < 0.05$ (Fig. 5C2 & E2). However, there was no significant difference between each size of CD20- and CD68-positive cells (Fig. 5B2 & D2).

Table 2
Immunohistochemical intensity staining scores in NMOSD, MS patients' and the controls' mucosa(Fromowitz method).

Group	NMOSD						MS			HCs					P
	1	2	3	4	5	6	1	2	3	1	2	3	4	5	
CD3	5	5	4	4	4	4	6	5	4	5	5	5	5	5	0.11
CD20	2	5	2	3	2	2	1	4	2	4	5	5	3	2	0.23
CD38	5	7	4	7	3	7	6	6	6	7	6	6	6	5	0.98
CD68	5	5	4	4	4	4	4	4	4	4	5	5	5	5	0.12
CD138	4	5	7	3	4	4	4	4	4	4	4	4	6	4	0.97
Notes: P-values for comparisons between NMOSD, MS and the controls, by K-W test.															

3.4 Intestinal mucosal dysbiosis in NMOSD patients

Our previous study showed that intestinal dysbiosis occurred in NMOSD patients by detecting the flora of faeces using 16S rRNA sequencing. To confirm this, we took examples of the colonic mucosa to detect 16S rRNA sequencing in the present study. The results are shown in Fig. 6. Taxonomic classification at the phylum level revealed that the intestinal mucosal bacteria of these subjects mainly consisted of *Firmicutes*, *Bacteroidetes*, and *Proteobacteria* (Fig. 6A). Based on the weighted UniFrac distance of 16S rRNA sequence profiles, the PCoA showed that the three groups generally clustered separately and that the diversity of the three groups was significantly different (Fig. 6B, P = 0.015 < 0.05, PERMANOVA test). LEfSe and Metastats algorithms were employed to identify the differential distribution of microbiota between NMOSD, MS and HC subjects. Two genera, *Granulicatella* and *Faecalibacterium*, were found to be differentially distributed between NMOSD and HC subjects by LEfSe analysis (LDA Score(log 10) = 4) (Fig. 6C). Thirty-eight differentially distributed genera were identified by Metastats analysis between the NMOSD and HC groups ($p < 0.05$). Combined with LEfSe results, we checked the quantitative analysis of *Granulicatella* abundance, again by Metastats, and revealed a significantly higher level in NMOSD patients (Fig. 6D, NMOSD vs HC, $p = 0.0028$; NMOSD vs MS, $p = 0.0136$). In this process, *Faecalibacterium* was excluded because it is a butyric acid-producing bacterium, which is considered a beneficial bacterium. On the basis of our previous faecal microbiota results[9], we paid attention to *Streptococcus*. Interestingly, the results are consistent with differences in *Streptococcus* in faecal microbiota previously published by our group, and the abundance of *Streptococcus* increased in NMOSD patients (Fig. 6E, NMOSD vs HC, $p = 0.023$, NMOSD vs MS, $p = 0.039$).

Discussion

To the best of our knowledge, the present study is the first report regarding changes in the intestinal mucosal barrier and mucosal microbiota of NMOSD patients. In this study, we found a wider cellular space of the epithelia of the colonic sigmoid mucosa, accompanied by the degradation of TJ protein and activation of T lymphocytes, eosinophils and plasma cells in the lamina propria in the sigmoid mucosa. In addition, intestinal mucosal dysbiosis with dominant harmful bacteria, *Streptococcus* and *Granulicatella*, may contribute to intestinal inflammation in NMOSD patients. Therefore, interruption of the intestinal mucosal barrier may open the door to allow harmful bacteria and their toxins into the blood and stimulate the pathogenesis of NMOSD.

As shown in NMOSD, defects in ZO-1, OCC and CLA expression could lead to abnormal permeability by increasing paracellular permeability[24–27], and the deepened intercellular space further demonstrates abnormal interepithelial junctions. TJ proteins are key molecules for maintaining the gut barrier and blood-brain barrier (BBB) that could increase the invasion of pro-inflammatory products. Perturbed gut integrity and permeability may lead to microbial (bacterial) translocation, and the eventual leakage of bacteria or their metabolites into the circulation can make the host susceptible to various types of diseases by inducing chronic or acute inflammatory responses[28]. This chronic inflammation may initiate NMOSD pathology through the broken BBB simultaneously or consecutively.

We found a chronic inflammatory response and activated inflammatory cells in all of the mucous membranes, although we did not observe an increased number of inflammatory cells compared to those in the HCs. CD138 (syndecan-1), which is upregulated during maturation of antibody-secreting cells, is required in a cell-intrinsic manner to mount an effective long-term humoural immune response following immunization[28] and may be related to the production of pathogenic AQP4-IgG in NMOSD. Changes in inflammatory cell function render these cells poor killers of bacteria but potent producers of inflammatory cytokines, which ultimately contributes to the inflammatory state[30]. Under normal circumstances, translocating microbes and microbial products will be endocytosed within the lamina propria and mesenteric lymph nodes[31]. However, if the host mucosal immune system is compromised, these defence mechanisms may fail, thus permitting the evasion and survival of bacteria at distant, extraintestinal sites[31, 32].

Consistent with our previous faecal microbiota study[9], the present study has also shown that *Streptococcus* is increased in sigmoid mucosa microbiota. Overabundance of *Streptococcus* and streptococcal toxin may elicit pro-inflammatory AQP4-specific T-cell and B-cell responses that contribute to the development of NMOSD. This result further supported the finding that *Streptococcus* may play a significant role in the pathogenesis of NMOSD. In addition, *Granulicatella* was also abundant in NMOSD, which may also contribute to intestinal inflammation because it has been reported to participate in several inflammatory diseases, such as periodontitis[33], caries[34], and endocarditis[35].

There are several limitations in our study. First, we enrolled only 6 NMOSD patients owing to the difficulty of sample collection and low incidence of NMOSD. Second, we observed activation of $CD138^{+}$ plasmocytes in NMOSD; however, functional experiments are needed to confirm their role. Last, our study

could not explain the causal relationship between the colonic mucosa microbiota, physical barrier, and immune response in NMOSD.

Conclusions

In conclusion, NMOSD patients had a disrupted intestinal barrier and intestinal mucosal microbiota dysbiosis. A study with a larger sample size is worthy of being performed in the future.

Abbreviations

NMOSD: Neuromyelitis optica spectrum disorder; MS: Multiple Sclerosis; HCs: Healthy controls; AQP4: aquaporin-4; CNS: central nervous system; BMI: body mass index; EDSS: Expanded Disability Status Scale; SP: streptavidin–biotin–peroxidase; EM: eletron microscope; TEM: transmission electron microscope; TJ: tight junction; AJ: adherent junction; Des: desmosomes; ZO-1: zonula occludens-1; OCC: occludin; CLA: claudin-1; AOD: average optical density; OTU: operational taxonomic unit; PCoA: Principal coordinate analysis; LDA: linear discriminant analysis; LEfSe: the linear discriminant analysis effect size; BBB: blood-brain barrier.

Declarations

Acknowledgments

The authors thank Dr Xianyi Lin for the help of fiber colonoscopy operation to the volunteers.

Fundings

This study was supported by research grants from the Natural Science Foundation of China (81771300) and Guangzhou Science and Technology Project, China (201904010444).

Availability of data and materials

The datasets generated during and/or analysed during the current study are available from the corresponding author upon reasonable request and with permission of the Third Affiliated Hospital of Sun Yat-sen University.

Authors' contributions

CC and ST contributed to the analysis and interpretation of data, drafting of the manuscript, statistical analysis, and technical and material support. LT was involved in participant enrolment and technical and material support. JG, YC, YW, and FP were involved in technical support and participant enrolment. LT and JG contributed to the analysis and interpretation of data and technical support. YR was involved in the study concept and design, critical revision of the manuscript, procurement of funding, study supervision, and final approval of the version to be published. WQ contributed to study supervision, participant enrolment, and critical revision of the manuscript. All authors read and approved the final version of the manuscript.

Ethics approval and consent to participate

For all volunteers, a written informed consent for fibercoloscope and the use of the material and clinical information for research purposes has been obtained from the donor or the next of kin. Donation procedures of sigmoid mucosa for scientific research purposes by the colono-fiberscopy have been approved by the ethics committee of the Third Affiliated Hospital of Sun Yat-sen University, Ethical approval number is [2019]02-418-01.

Consent for publication

Not applicable.

Competing interests

The authors declare no financial or other conflicts of interest.

References

1. Varrin-Doyer M, Spencer CM, Schulze-Topphoff U, Nelson PA, Stroud RM, Cree BA, Zamvil SS. Aquaporin 4-specific T cells in neuromyelitis optica exhibit a Th17 bias and recognize Clostridium ABC transporter. Ann Neurol. 2012;72:53–64.
2. Camara-Lemarroy CR, Metz LM, Yong VW. Focus on the gut-brain axis: Multiple sclerosis, the intestinal barrier and the microbiome. World J Gastroentero. 2018;24:4217–23.
3. Smith PM, Howitt MR, Panikov N, Michaud M, Gallini CA, Bohlooly-Y M, Glickman JN, Garrett WS. The microbial metabolites, short-chain fatty acids, regulate colonic Treg cell homeostasis. Science. 2013;341:569–73.
4. Odenwald MA, Turner JR. The intestinal epithelial barrier: a therapeutic target? Nat Rev Gastroenterol Hepatol. 2017;14:9–21.

5. Mizoguchi A, Mizoguchi E. Inflammatory bowel disease, past, present and future: lessons from animal models. J Gastroenterol. 2008;43:1–17.
6. Parthasarathy G, Chen J, Chen X, Chia N, O'Connor HM, Wolf PG, Gaskins HR, Bharucha AE. Relationship Between Microbiota of the Colonic Mucosa vs Feces and Symptoms, Colonic Transit, and Methane Production in Female Patients With Chronic Constipation. Gastroenterology. 2016;150:367–79.
7. Altomare A, Putignani L, Del CF, Cocca S, Angeletti S, Ciccozzi M, Tripiciano C, Dalla PB, Cicala M, Guarino M. Gut mucosal-associated microbiota better discloses inflammatory bowel disease differential patterns than faecal microbiota. Dig Liver Dis. 2019;51:648–56.
8. Zeng Q, Junli G, Liu X, Chen C, Sun X, Li H, Zhou Y, Cui C, Wang Y, Yang Y, et al. Gut dysbiosis and lack of short chain fatty acids in a Chinese cohort of patients with multiple sclerosis. Neurochem Int. 2019;129:104468.
9. Gong J, Qiu W, Zeng Q, Liu X, Sun X, Li H, Yang Y, Wu A, Bao J, Wang Y, et al. Lack of short-chain fatty acids and overgrowth of opportunistic pathogens define dysbiosis of neuromyelitis optica spectrum disorders: A Chinese pilot study. Mult Scler. 2019;25:1316–25.
10. Jangi S, Gandhi R, Cox LM, Li N, von Glehn F, Yan R, Patel B, Mazzola MA, Liu S, Glanz BL, et al. Alterations of the human gut microbiome in multiple sclerosis. Nat Commun. 2016;7:12015.
11. Rothhammer V, Quintana FJ. Environmental control of autoimmune inflammation in the central nervous system. Curr Opin Immunol. 2016;43:46–53.
12. Wingerchuk DM, Banwell B, Bennett JL, Cabre P, Carroll W, Chitnis T, de Seze J, Fujihara K, Greenberg B, Jacob A, et al. International consensus diagnostic criteria for neuromyelitis optica spectrum disorders. Neurology. 2015;85:177–89.
13. Thompson AJ, Banwell BL, Barkhof F, Carroll WM, Coetzee T, Comi G, Correale J, Fazekas F, Filippi M, Freedman MS, et al. Diagnosis of multiple sclerosis: 2017 revisions of the McDonald criteria. Lancet Neurol. 2018;17:162–73.
14. Lepage P, Seksik P, Sutren M, de la Cochetiere MF, Jian R, Marteau P, Dore J. Biodiversity of the mucosa-associated microbiota is stable along the distal digestive tract in healthy individuals and patients with IBD. Inflamm Bowel Dis. 2005;11:473–80.
15. Naftali T, Reshef L, Kovacs A, Porat R, Amir I, Konikoff FM, Gophna U. Distinct Microbiotas are Associated with Ileum-Restricted and Colon-Involving Crohn's Disease. Inflamm Bowel Dis. 2016;22:293–302.
16. Ma Y, Ma L, Guo Q, Zhang S. Expression of bone morphogenetic protein-2 and its receptors in epithelial ovarian cancer and their influence on the prognosis of ovarian cancer patients. J Exp Clin Cancer Res. 2010;29:85.
17. Magoc T, Salzberg SL. FLASH: fast length adjustment of short reads to improve genome assemblies. Bioinformatics. 2011;27:2957–63.
18. Bolger AM, Lohse M, Usadel B. Trimmomatic: a flexible trimmer for Illumina sequence data. Bioinformatics. 2014;30:2114–20.

19. Edgar RC, Haas BJ, Clemente JC, Quince C, Knight R. UCHIME improves sensitivity and speed of chimera detection. Bioinformatics. 2011;27:2194–200.
20. Segata N, Izard J, Waldron L, Gevers D, Miropolsky L, Garrett WS, Huttenhower C. Metagenomic biomarker discovery and explanation. Genome Biol. 2011;12:R60.
21. White JR, Nagarajan N, Pop M. Statistical methods for detecting differentially abundant features in clinical metagenomic samples. Plos Comput Biol. 2009;5:e1000352.
22. Edgar RC. Search and clustering orders of magnitude faster than BLAST. Bioinformatics. 2010;26:2460–1.
23. Krzysciak W, Pluskwa KK, Jurczak A, Koscielniak D. The pathogenicity of the Streptococcus genus. Eur J Clin Microbiol Infect Dis. 2013;32:1361–76.
24. Furuse M, Itoh M, Hirase T, Nagafuchi A, Yonemura S, Tsukita S, Tsukita S. Direct association of occludin with ZO-1 and its possible involvement in the localization of occludin at tight junctions. J Cell Biol. 1994;127:1617–26.
25. Bauer H, Zweimueller-Mayer J, Steinbacher P, Lametschwandtner A, Bauer HC. The dual role of zonula occludens (ZO) proteins. J Biomed Biotechnol. 2010;2010:402593.
26. Umeda K, Matsui T, Nakayama M, Furuse K, Sasaki H, Furuse M, Tsukita S. Establishment and characterization of cultured epithelial cells lacking expression of ZO-1. J Biol Chem. 2004;279:44785–94.
27. Bertiaux-Vandaele N, Youmba SB, Belmonte L, Lecleire S, Antonietti M, Gourcerol G, Leroi AM, Dechelotte P, Menard JF, Ducrotte P, Coeffier M. The expression and the cellular distribution of the tight junction proteins are altered in irritable bowel syndrome patients with differences according to the disease subtype. Am J Gastroenterol. 2011;106:2165–73.
28. Nagpal R, Yadav H. Bacterial Translocation from the Gut to the Distant Organs: An Overview. Ann Nutr Metab. 2017;71(Suppl 1):11–6.
29. McCarron MJ, Park PW, Fooksman DR. CD138 mediates selection of mature plasma cells by regulating their survival. Blood. 2017;129:2749–59.
30. Okumura R, Takeda K. Maintenance of intestinal homeostasis by mucosal barriers. Inflamm Regen. 2018;38:5.
31. Alexander JW, Gianotti L, Pyles T, Carey MA, Babcock GF. Distribution and survival of Escherichia coli translocating from the intestine after thermal injury. Ann Surg. 1991;213:558–66, 566–567.
32. Thevaranjan N, Puchta A, Schulz C, Naidoo A, Szamosi JC, Verschoor CP, Loukov D, Schenck LP, Jury J, Foley KP, et al. Age-Associated Microbial Dysbiosis Promotes Intestinal Permeability, Systemic Inflammation, and Macrophage Dysfunction. Cell Host Microbe. 2018;23:570.
33. Belstrom D, Fiehn NE, Nielsen CH, Kirkby N, Twetman S, Klepac-Ceraj V, Paster BJ, Holmstrup P. Differences in bacterial saliva profile between periodontitis patients and a control cohort. J Clin Periodontol. 2014;41:104–12.

34. Kanasi E, Dewhirst FE, Chalmers NI, Kent RJ, Moore A, Hughes CV, Pradhan N, Loo CY, Tanner AC. Clonal analysis of the microbiota of severe early childhood caries. Caries Res. 2010;44:485–97.
35. Siqueira JJ, Rocas IN. Catonella morbi and Granulicatella adiacens: new species in endodontic infections. Oral Surg Oral Med Oral Pathol Oral Radiol Endod. 2006;102:259–64.

Figures

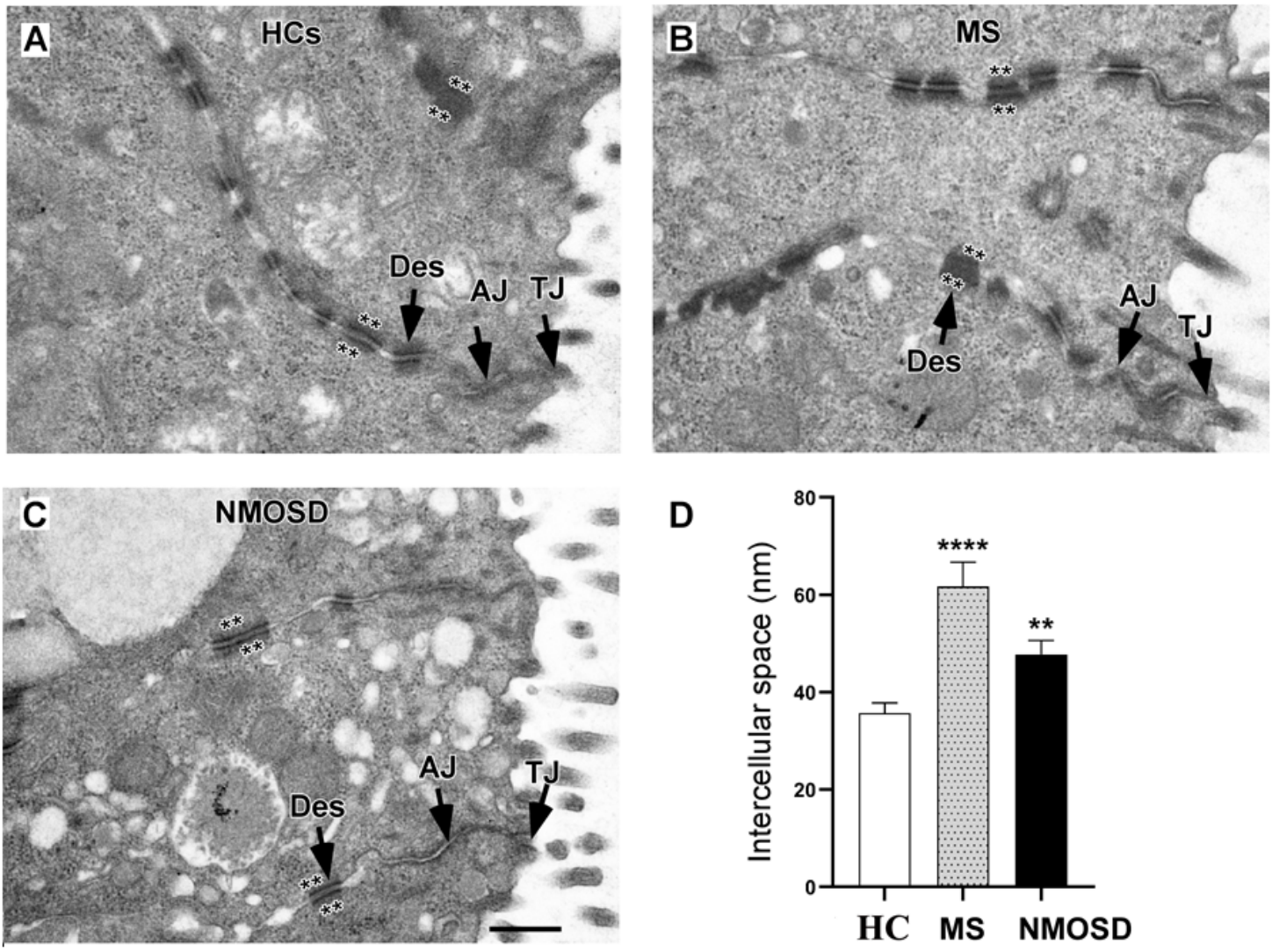

Figure 1

EM photos and histogram showing changes in intercellular spaces of the epithelium. Under TEM, three types of intercellular junctions can be found between the epithelium of colonic mucosa (A, B & C). Examples of a TJ, AJ and desmosome (Des) are shown in an HC subject (A) and in MS (B) and NMOSD (C) patients. From EM photos, we found that some TJs in NMOSD patients were separated between two adjacent epithelia (C, arrow) and that the dense plates on each side of a Des became pale compared to those in the HC and MS groups (A, B & C, asterisks). Quantitative data show that the intercellular space of

these junctions becomes wider in MS and NMOSD patients than in the HC group (D, **p<0.01, ****p<0.0001). Scale bar (500 nm) in C is equal to A & B.

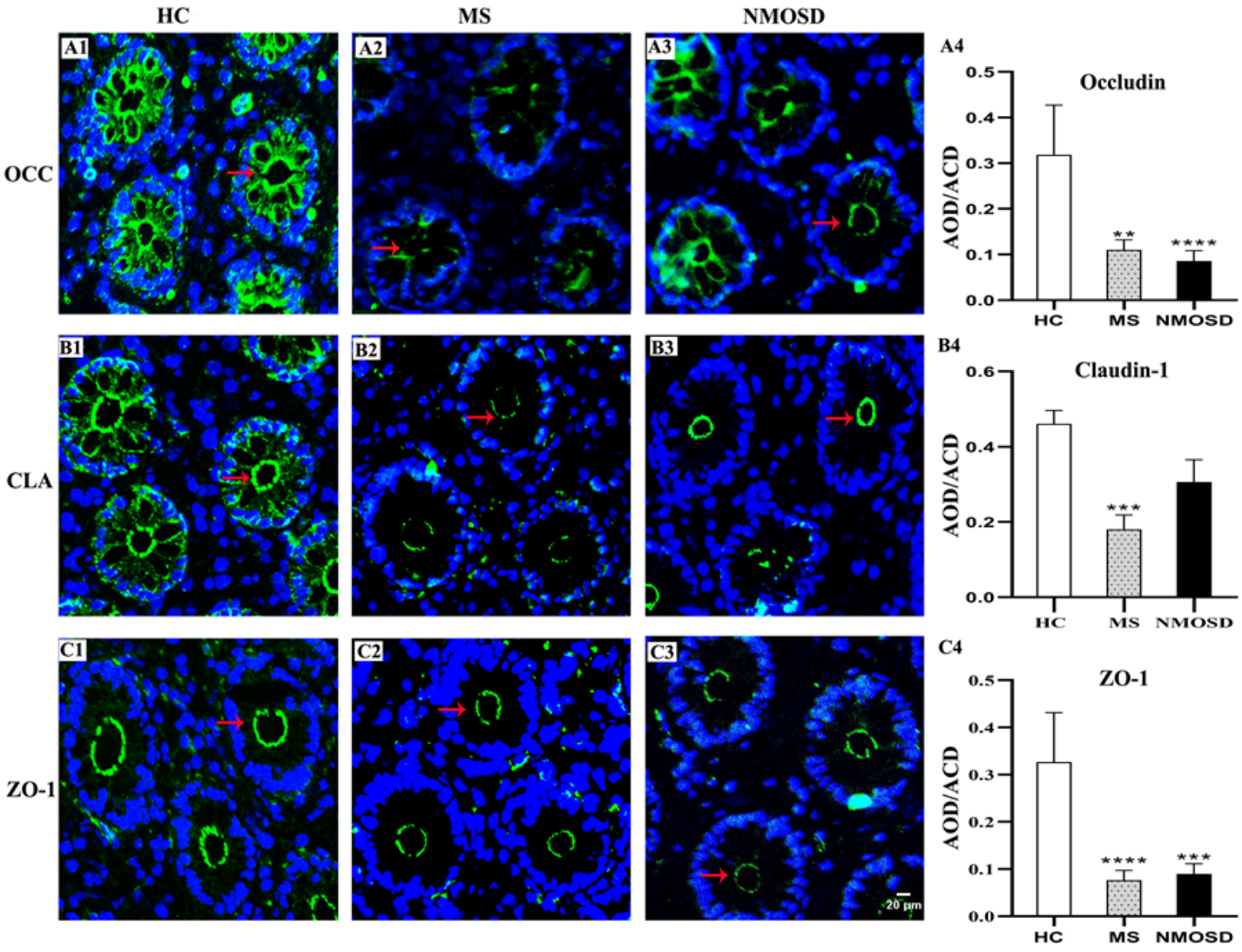

Figure 2

Photomicrograph and histogram showing changes in TJ proteins of the colonic mucosa. Positive immunostaining (arrows, green) for OCC, CLA and ZO-1 of the sigmoid colonic mucosa in HC, MS and NMOSD groups is seen in A1-A3, B1-B3, and C1-C3. The nuclei of the epithelium were counterstained with DAPI (blue). The results of quantitative analysis of OCC, CLA and ZO-1 are found in A4, B4 and C4, respectively. **p<0.01, ***p<0.001, ****p<0.0001 when compared with the control group. OCC: occludin; CLA: claudin-1; ZO-1: zonula occludens-1; AOD: average optical density. The scale bar (20μm) in C3 is equal to A1-A3, B1-B3 and C1-C3.

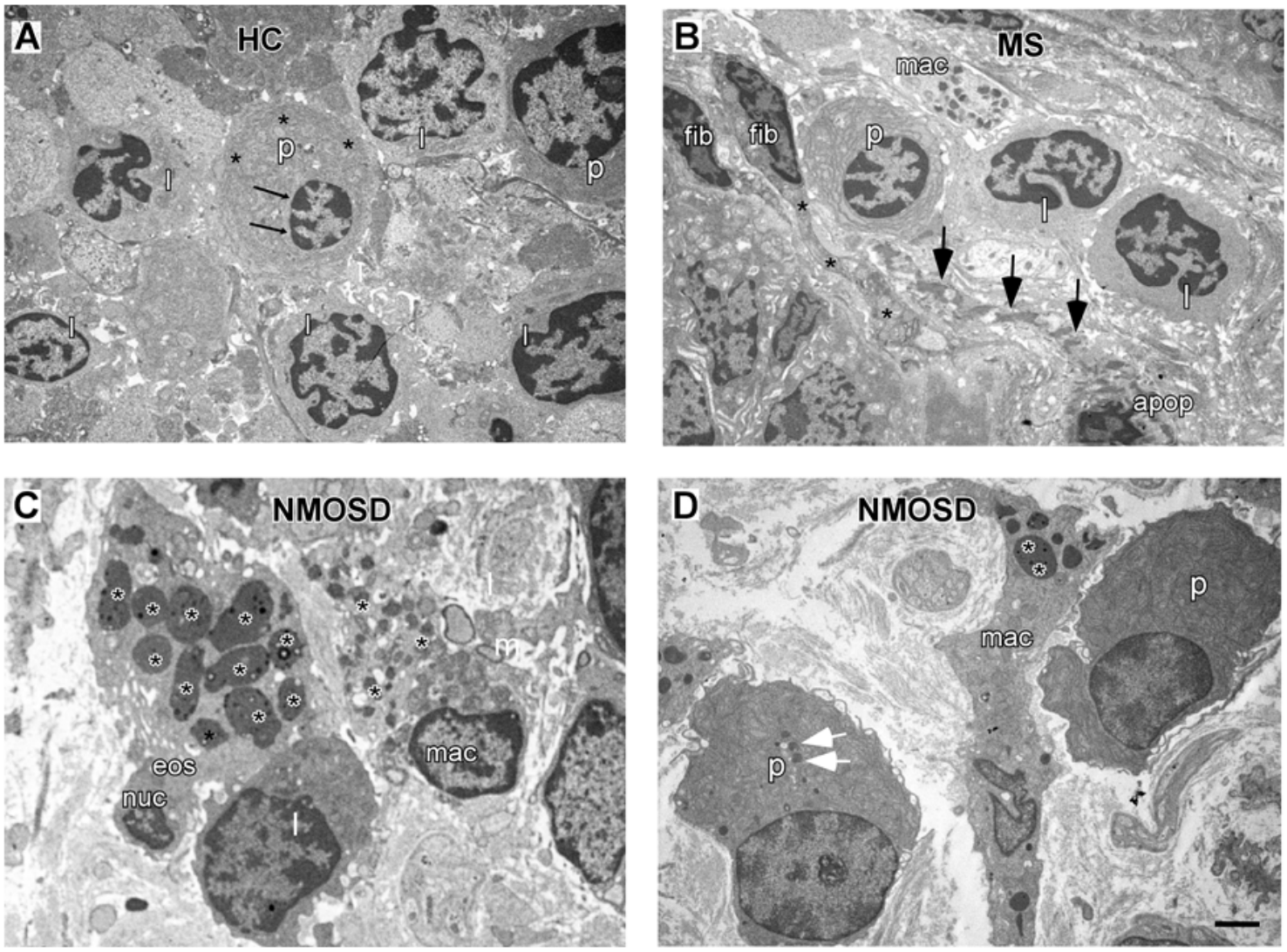

Figure 3

EM photos showing changes in the morphology of interstitial inflammatory cells in the lamina proper. l, lymphocyte; p, plasmocyte; mac, macrophage; fib, fibrocyte; apop, apoptotic fibrocyte; eos, eosinophil. The scale bar (2 μm) in D is equal to A, B and C.

Figure 4

Photomicrographs showing the immunohistochemical staining for inflammatory cell markers using the DAB visualization method. These markers include CD3 (a marker for T cells, A1, A2, & A3), CD20 (a marker for B cells, B1, B2 & B3), CD38 (markers for activated lymphocytes and plasmocytes, C1, C2 & C3), CD68 (a marker for microphage, D1, D2 & D3) and CD138 (a marker for plasmocytes, E1, E2 & E3). The positive staining is brown in colour (black arrows). All slides were counterstained with haematoxylin (blue). The scale bar (100 μm) in E3 is equal to all photos.

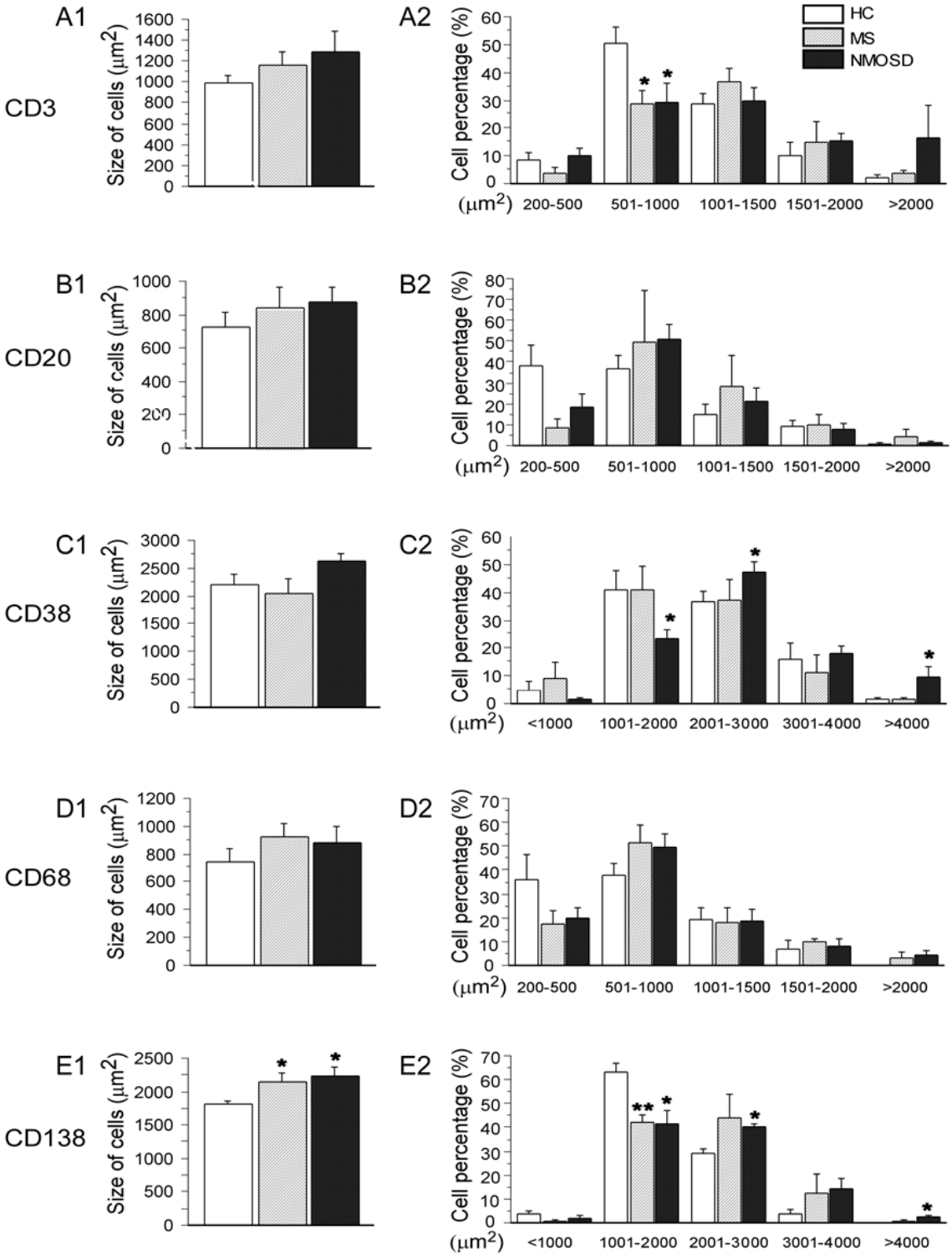

Figure 5

Histogram showing changes in the size of CD3-, CD20-, CD38-, CD68-, and CD138-positive cells. The left column indicates the mean area of total cells, and the right column shows the percentage of cells of different sizes. *p< 0.05, **p < 0.01 when compared with the control group.

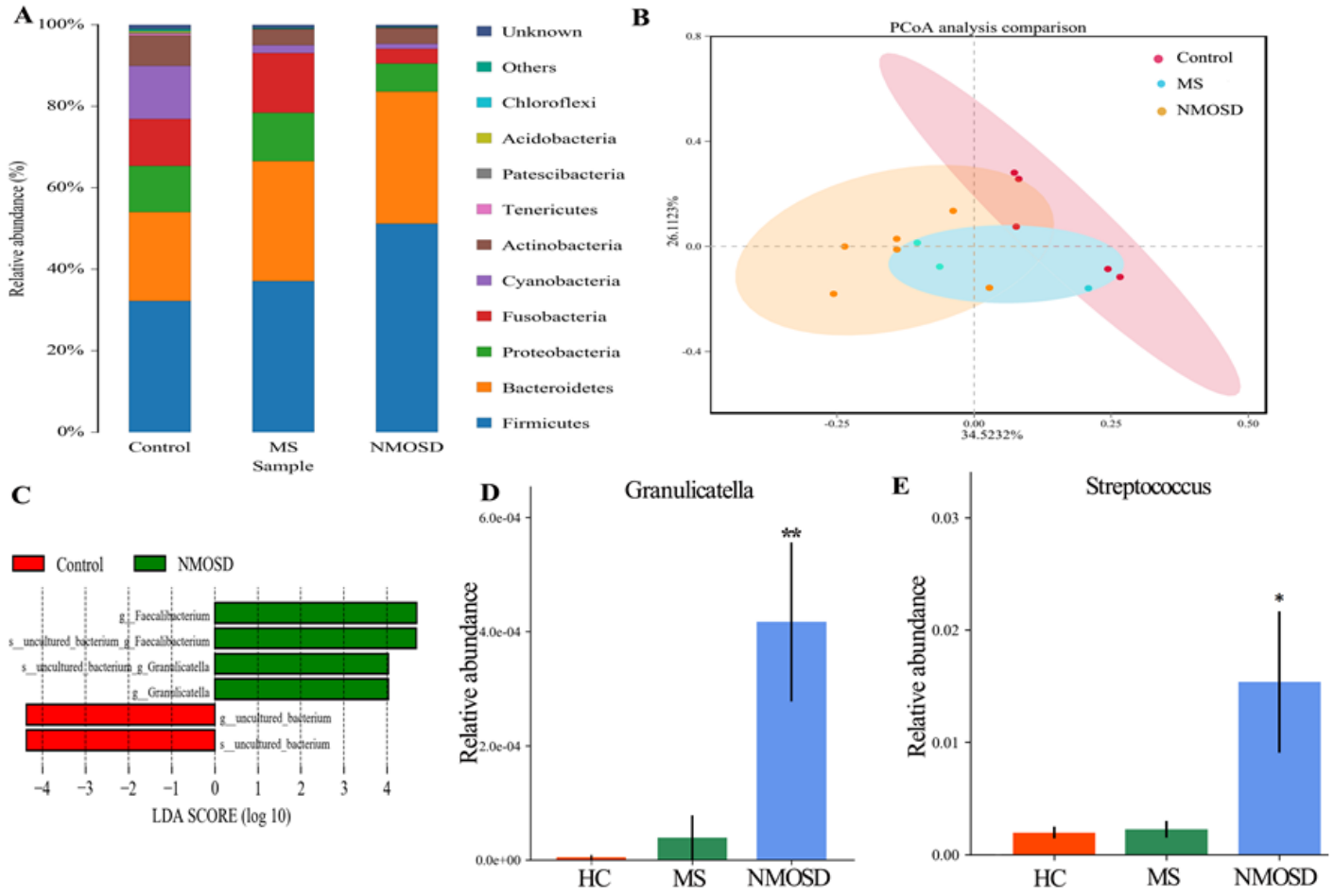

Figure 6

Histogram and scatter diagram showing the distribution characteristics of the intestinal microbiota among the three groups. (A) The distribution characteristics of the intestinal microbiota of the colonic mucosa at the phylum level from the same species. (B) The result of PCoA analysis illustrating the grouping patterns between NMOSD, MS patients and controls ($p < 0.05$, PERMANOVA test). Each point represents the composition of the intestinal microbiota of one participant. (C) Based on LEfSe, the phylogenetic distribution of intestinal mucosal bacteria associated with NMOSD comprised mainly Faecalibacterium and Granulicatella (green). LDA scores revealed a significant bacterial difference between the three groups (LDA score (log 10) = 4), with uncultured bacteria in HC (red) subjects and no differential bacteria in MS patients. (D) The relative abundance of Granulicatella in participants from the three groups (NMOSD vs HC; *$p<0.01$, Metastats analysis). (E) Comparing the relative abundances of Streptococcus among the three groups (NMOSD vs HCs; NMOSD vs MS; *$p<0.05$, Metastats analysis).